Supporting information

Hierarchical $MnCo_2O_4$ Nanowire@NiFe Layered Double Hydroxide Nanosheets Heterostructures on Ni foam for Overall Water Splitting

Huafeng Shi, Kun Yang, Fangfang Wang, Yonghong Ni* and Muheng Zhai

College of Chemistry and Materials Science, Key Laboratory of Functional Molecular Solids, Ministry of Education, Anhui Laboratory of Molecule-Based Materials, Anhui Key Laboratory of Functional Molecular Solids, Anhui Normal University, 189 Jiuhua Southern Road, Wuhu, 241002, PR China

Materials characterization: Field emission scanning electron microscopy (FESEM, Hitachi S-4800) and transmission electron microscopy (TEM, Hitachi HT7700) were utilized to analyze the morphology and structure of the materials. The EDS elemental mapping images of the final product were obtained from Bruker Nano Analytics (GmbH Berlin, Germany) with the operated voltage of 200 kV. X-ray diffraction (XRD, Bruker D8 ADVANCE) was used to characterize the crystal structure. X-ray photoelectron spectroscopy (XPS) spectrum of catalysts was acquired by using a Thermo ESCALAB 250 instrument.

Electrochemical measurement: A CHI 660E electrochemical workstation was utilized for all electrochemical measurements. The carbon rod and Hg/HgO were used as the counter electrode and reference electrode, respectively. The MCO@NiFe-LDH/NF, $MnCo_2O_4$/NF or NiFe LDH/NF was separately used as the working electrode, employing 1 M KOH solution as the electrolyte. For OER performance measurement, all linear sweep voltammograms (LSV) were collected from 0.2

to 0.8 V (vs. saturated Hg/HgO) at a scan rate of 5 mV s^{-1} with 90% IR compensation. The stability test was carried out through chronopotentiometry measurements without IR compensation at corresponding potentials to deliver current densities of 20, 50 and 100 mA cm^{-2} for 20 h, respectively. The electrochemical impedance spectroscopy (EIS) measurements were recorded in the frequency range from 10^{-2} Hz to 10^{5} Hz with amplitude of 5 mV at the overpotential of 300 mV. The electrochemically active surface area (ECSA) was estimated from the electrochemical double-layer capacitance (C_{dl}) obtained by cyclic voltammograms (CVs), which were measured in the potential range of 0.15-0.25 V (vs. saturated Hg/HgO) without faradic reaction at different scan rates (10, 20, 30, 40, 50 mV s^{-1}). The Turnover frequency (TOF) values were calculated from the equation: $TOF = (j \times A)/(4 \times n \times F)$. Where, j is the current density at a certain overpotential, A is the surface area of the electrode, F is the Faraday constant (96485 C mol^{-1}) and n is the molar number of active sites.

For HER performance measurement, the LSV curves were performed from -0.9 to -1.4 V (vs. saturated Hg/HgO) at a scan rate of 5 mV s^{-1} with 90% IR compensation. The EIS spectra were obtained in the frequency range from 10^{-2} to 10^{5} Hz at the overpotential of -200 mV.

To investigate the overall water splitting performances of various electrodes (MCO@NiFe-LDH/NF, $MnCo_2O_4$/NF, NiFe LDH/NF and NF), the LSV curves were measured in 1 M KOH solution at a scan rate of 5 mV s^{-1} from 1.0 to 2.0 V with 90% IR compensation. The long-term stability performance was performed at the current density of 50 mA cm^{-2} for 200 h or 100 mA cm^{-2} for 50 h.

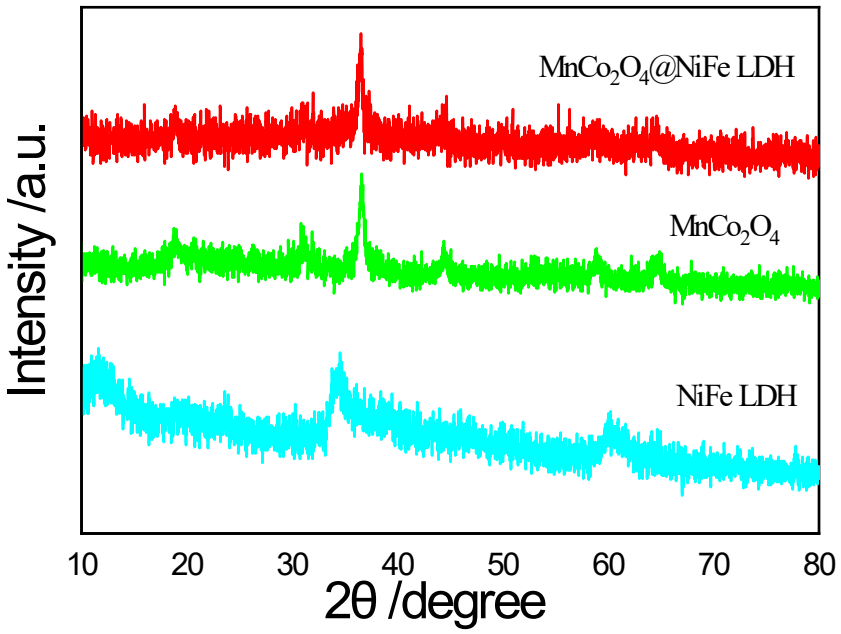

Figure S1. XRD patterns of as-obtained $MnCo_2O_4$, NiFe LDH and MCO@NiFe-LDH.

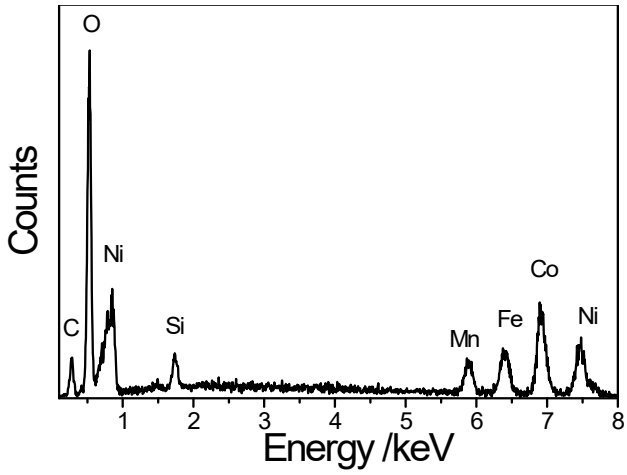

Figure S2. EDS analysis of as-prepared MCO@NiFe-LDH nanowires array.

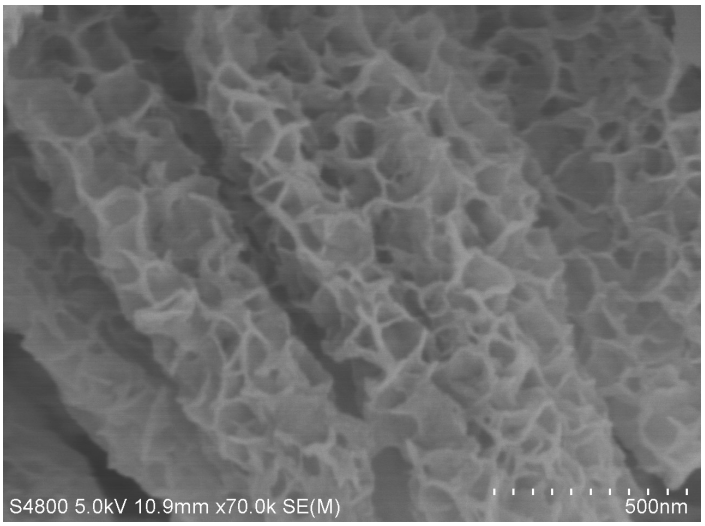

Figure S3. A representative FESEM image of MCO@NiFe-LDH catalyst after continuously catalyzing OER for 20 h at the current density of 100 mA cm^{-2}.

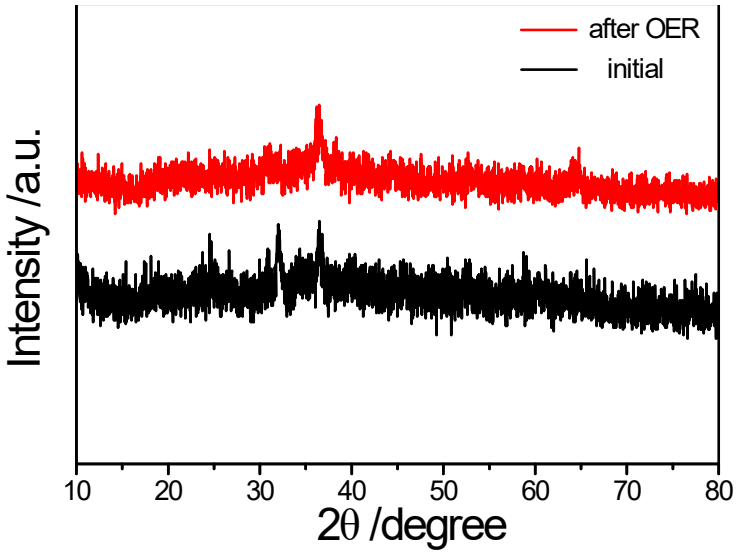

Figure S4. The XRD patterns of MCO@NiFe-LDH catalyst before and after continuously catalyzing for 20 h at the current density of 100 mA cm^{-2} for OER.

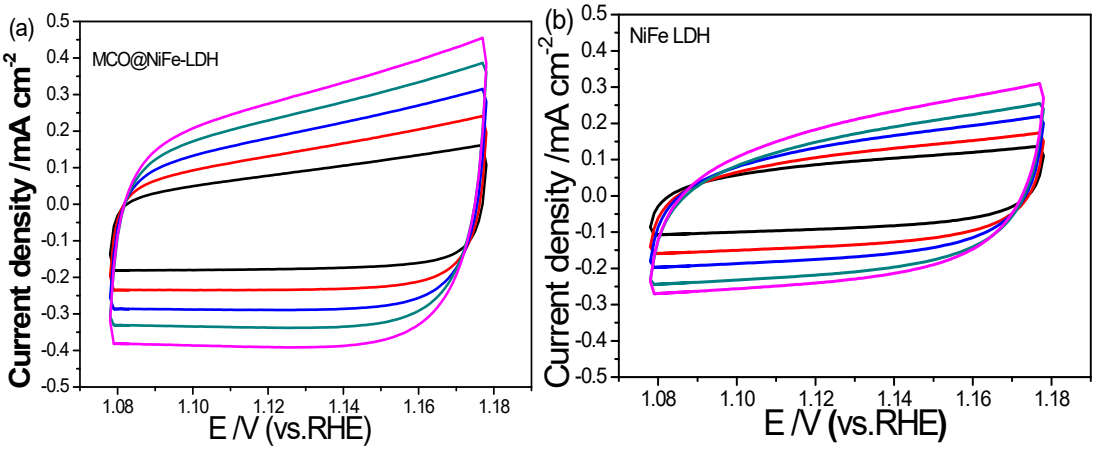

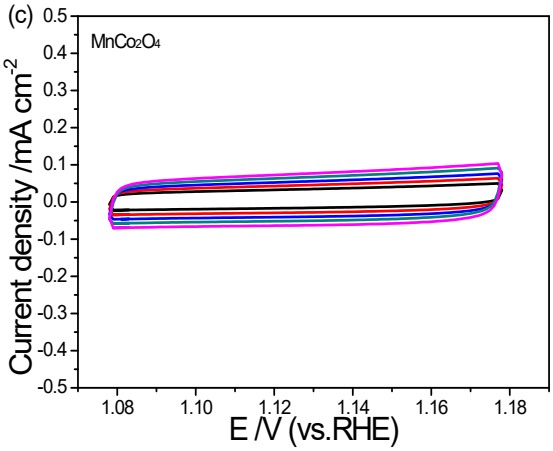

Figure S5. The cyclic voltammograms of various electrodes at different scan rates of 20, 30, 40, 50 and 60 mV s^{-1}: (a) MCO@NiFe-LDH/NF, (b) NiFe LDH/NF and (c) $MnCo_2O_4$/NF.

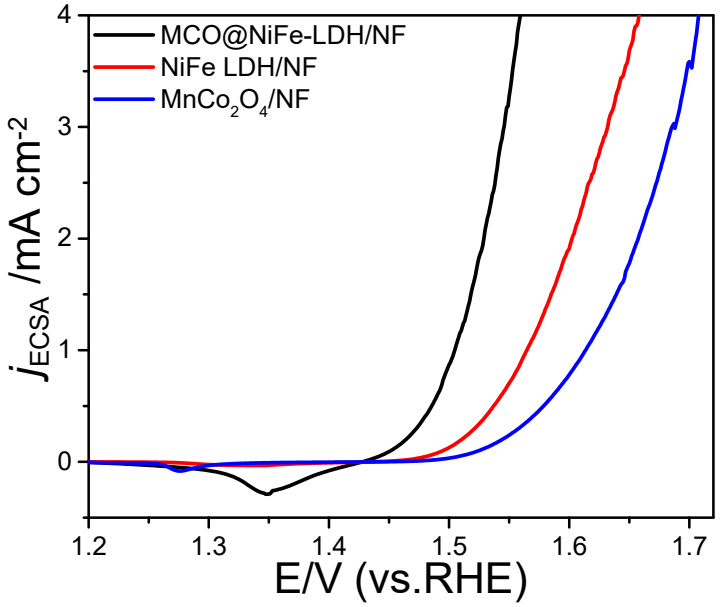

Figure S6. The ECSA-normalized LSV curves of various electrodes for OER.

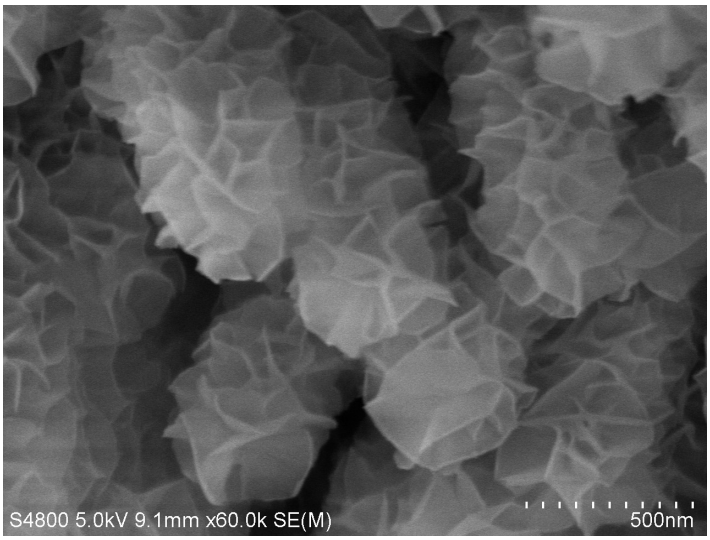

Figure S7. A typical FESEM image of MCO@NiFe-LDH catalyst after continuously catalyzing HER for 20 h at the current density of 100 mA cm^{-2}.

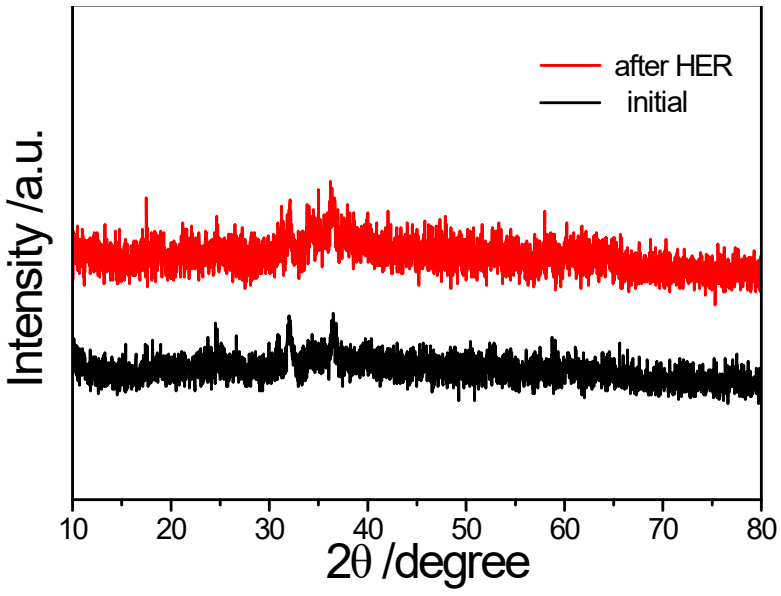

Figure S8. The XRD patterns of MCO@NiFe-LDH catalyst before and after continuously catalyzing for 20 h at the current density of 100 mA cm^{-2} for HER.

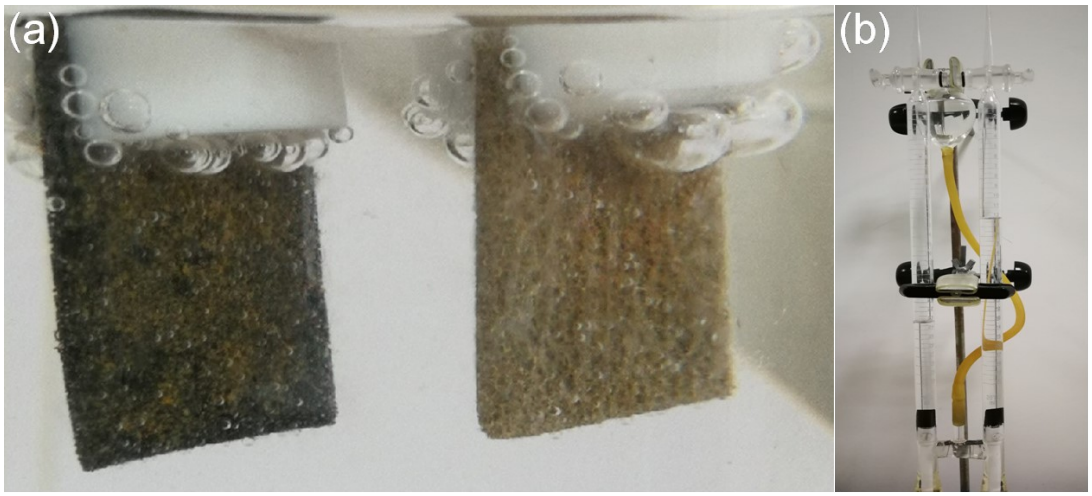

Figure S9. (a) Digital photograph for overall water splitting using the MCO@NiFe-LDH/NF electrode as both anode and cathode; and (b) the Hoffman device.

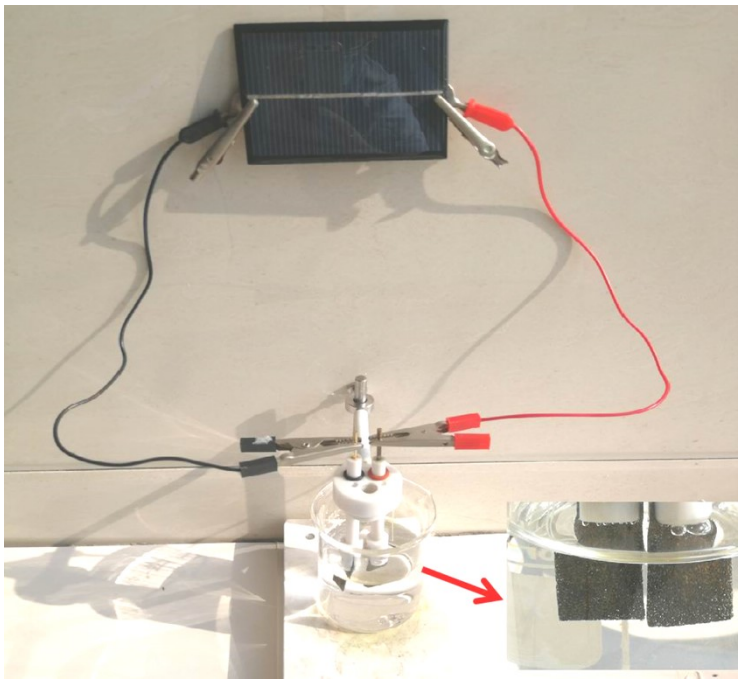

Figure S10. A photograph of the overall water splitting driven by a commercial polycrystalline silicon solar cell of 1.5 V under Sunlight irradiation.

Table S1. The comparison of OER catalytic performance of $MnCo_2O_4$@NiFe LDH with some OER catalysts reported in the literature.

Catalyst	Electrolyte	η (mV) **at 10 mA cm^{-2}**	Ref.
$MnCo_2O_4$@NiFe LDH/NF	1M KOH	215	This work
NiFe LDH/NF	1M KOH	271	This work
$MnCo_2O_4$/NF	1M KOH	301	This work
$NiCo_2S_4$/NF	1M KOH	260	1
$Co(OH)_2$	1M KOH	360	2
$NiO/NiFe_2O_4$	1M KOH	302	3
$NiO\text{-}NiFe_2O_4$/rGO	1M KOH	296	4
$Ni(OH)_2$	1M KOH	595	5
Co_3S_4	1M KOH	355	6
Ni_3S_2/MnO_2	1M KOH	260	7
CuOx@CoO	1M KOH	254	8
Mn-CoN	1M KOH	265	9
Co−Se−S−O/CC	1M KOH	480	10

Table S2. The solution resistance (R_s), charge transfer resistance (R_{ct}) and mass transfer resistance (R_f) of various working electrodes.

Electrode	R_s /Ω	R_{ct} /Ω	R_f /Ω
MCO@NiFe-LDH/NF	1.02	2.95	6.53
NiFe LDH/NF	1.44	21.48	19.64
$MnCo_2O_4$/NF	1.48	31.53	14.24

Table S3. The comparison of HER catalytic performance of $MnCo_2O_4$@NiFe LDH with some HER catalysts reported in the literature.

Catalyst	Electrolyte	η (mV) **at 10 mA cm^{-2}**	Ref.
$MnCo_2O_4$@NiFe LDH/NF	1M KOH	129	This work
$MnCo_2O_4$/NF	1M KOH	220	This work
NiFe LDH/NF	1M KOH	193	This work
Ni_3S_2/NF	1M KOH	223	11
NiCoS	1M KOH	228	12
NiCoP	1M KOH	197	13
FeP	1M KOH	370	14
$MoSe_2/CoSe_2$	1M KOH	148	15
Ni_3S_2/MnO_2/NF	1 M KOH	102	16
CoP/NPC/TF	1 M KOH	91	17
Mn-Co-P/Ti	1 M KOH	76	18
Mn-CoP	1 M KOH	81	19
Co_9S_8/NC@MoS_2	1 M KOH	67	20

Table S4. The comparison of overall water splitting catalytic performance of $MnCo_2O_4$@NiFe LDH with some bifunctional catalysts reported in the literature.

Catalyst	Electrolyte	Full water splitting		Ref.
		Cell voltage (V) at **10 mA cm^{-2}**	η (mV) at **10 mA cm^{-2}**	
$MnCo_2O_4$@NiFe LDH/NF	1M KOH	1.55	330	This work
$MnCo_2O_4$/NF	1M KOH	1.73	500	This work
NiFe LDH/NF	1M KOH	1.64	410	This work
α-NiOOH/NF	1M KOH	1.66	430	21
VOOH	1M KOH	1.62	390	22
Co_9S_8	1M KOH	1.60	370	23
N doped Ni_3S_2/VS_2	1M KOH	1.65	418	24
Ni_2P/rGo	1M KOH	1.61	380	25
MoS_2/Ni_3S_2	1M KOH	1.56	330	26
NiFeRu-LDH	1M KOH	1.52	290	27
NiFeMo	1M KOH	1.45	220	28
Cu@NiFe -LDH	1M KOH	1.53	300	29
Fe-NiO	1M KOH	1.58	350	30

References

1 A. Sivanantham, P. Ganesan, S. Shanmugam, Adv. Funct. Mater. 2016, 26, 4661-4672.

2 L. Huang, J. Jiang, L. Ai, ACS Appl. Mater. Interfaces. 2017, 9, 7059-7067.

3 G. Liu, X. Gao, K. Wang, D. He, J. Li, Int. J. Hydrogen. Energy. 2016, 41, 17976-17986.

4 G. Zhang, Y. Li, Y. Zhou, F. Yang, Chem. Electro. Chem. 2016, 3, 1927-1936.

5 X. M. Zhou, Z. M. Xia, Z. Y. Zhang, Y. Y. Ma, Y. Q. Qu, J. Mater. Chem. A. 2014, 2, 11799-11806.

6 Y. W. Liu, C. Xiao, M. J. Lyu, Y. Lin, W. Z. Cai, P. C. Huang, W. Tong, Y. M. Zou, Y. Xie, Angew. Chem., Int. Ed. 2015, 54, 11231-11235.

7 .Y. Xiong, L. Xu, C. Jin, Q. Sun. J. Alloy Compd. 2020, 745, 468-478

8 P. Li, J. Wang, N. Cai, L. Wang, J. Tong, F. Yu, ChemCatChem. 2020, 12, 1639 – 1646

9 Y. Sun, T. Zhang, X. Li, D. Liu, G. Liu, X. Zhang, X. Lyu, W. Cai, Y. Li, Chem. Commun., 2017, 53, 13237--13240.

10 Z. M. Luo, J. W. Wang, J. B. Tan, Z. M. Zhang, T. B. Lu. ACS Appl. Mater. Interfaces 2018, 10, 8231−8237

11 L. L. Feng, G. T. Yu, Y. Y.Wu, G. D. Li, H. Li, Y. H. Sun, T. Asefa, W. Chen, X. X. Zou, J. Am. Chem. Soc. 2015, 137, 14023-14026.

12 D. X. Zhang, W. D. He, Z. Zhang, X. J. Xu, J. Alloy Compd. 2019, 785, 468-474.

13 J. Z. Li, G. D. Wei, Y. K. Zhu, Y. L. Xi, X. X. Pan, Y. Ji, Igor. V. Zatovsky, W. Han, J. Mater. Chem. A. 2017, 5, 14828-14837.

14 Y. H. Liang, Q. Liu, Abdullah M. Asiri, X. P. Sun, Y. L. Luo, ACS Catal. 2014, 4, 4065-4069.

15 X. Q. Wang, B. J. Zheng, B. Yu, B. Wang, W. Q. Hou, W. L. Zhang, Y. F. Chen, J. Mater. Chem. A 2018, 6, 7842-7850.

16 Y. Xiong, L. L. Xu, C. D. Jin, Q. F. Sun, Appl. Catal. B 2019, 254, 329-338.

17 X. Huang, X. Xu, C. Li, D. Wu, D. Cheng, D. Cao. Adv. Energy Mater. 2019, 1803970

18 Q. Zhang, C. C. Zhang, J. B. Liang, P. G. Yin, Y. Tian, ACS Sustain. Chem. Eng. 2017, 5, 3808-3818.

19 T. Liu, X. Ma, D. Liu, S. Hao, G. Du, Y. Ma, A. M. Asiri, X. Sun, L. Chen. ACS Catal. 2017, 7, 98−102.

20 D. Zhao, K. Wu, Z. Liu, Y. Liu, D. Wang, Q. Peng, C. Chen, Y. Li, Nano Energy 2019, 56,

411-419.

21 H. H. Shi, H. F. Liang, F. W. Ming, Z. C. Wang, Angew. Chem. Int. Ed. 2017, 56, 573-577.

22 Y. T. Zhang, S. J. Chao, X. B. Wang, H. J. Han, Z. Y. Bai, L. Yang, Electrochim. Acta. 2017, 246, 380-390.

23 X.W. Zhong, J. Tang, J. W. Wang, M. M. Shao, J. W. Chai, S. P. Wang, M. Yang, Y. Yang, N. Wang, S. J. Wang, B. M. Xu, H. Pan, Electrochim. Acta. 2018, 269, 55-61.

24 L. T. Yan, H. M. Jiang, Y. L. Xing, Y. Wang, D. D. Liu, X. B. Zhao, J. Mater. Chem. A. 2018, 6, 1682-1691.

25 J. Zhang, T. Wang, D. Pohl, B. Rellinghaus, R.H. Dong, S. H. Liu, X. D. Zhuang, X. L. Feng, Angew. Chem. Int. Ed. 2016, 55, 6702-6707.

26 G. B. Chen, T. Wang, J. Zhang, P. Liu, H. J. Sun, X. D. Zhuang, M. W. Chen, X. L. Feng, Adv. Mater. 2018, 30, 1706279.

27 F. Qin, Z. H. Zhao, M. K. Alam, Y. Z. Ni, F. Robles-Hernandez, L. Yu, S. Chen, Z. F. Ren, Z. M. Wang, J. M. Bao, ACS Energy Lett. 2018, 3, 546-554.

28 C. Xiao, Y. Li, X. Lu, C. Zhao, Adv. Funct. Mater. 2016, 26, 3515 – 3523

29 L. Yu, H. Zhou, J. Sun, F. Qin, F. Yu, J. Bao, Y. Yu, S. Chen, Z. Ren, Energy Environ. Sci., 2017, 10, 1820

30 Z. Wu, Z. Zou, J. Huang, F. Gao, J. Catal. 2018, 358, 243-252.